PAPER

Fabrication of ZIF-9@super-macroporous microsphere for adsorptive removal of Congo red from water†

Juan Dai,[a] Shangzhen Xiao,[a] Jing Liu,[a] Jing He,[a] Jiandu Lei*[b] and Luying Wang*[a]

A novel composite adsorbent of ZIF-9 nanoparticles growing on super-macroporous microspheres (SMM) was synthesized *via in situ* growth method for adsorptive removal of Congo red from water. The as-synthesized ZIF-9@SMM adsorbent was characterized by XRD, SEM, and BET experiments, and the results showed the ZIF-9 nanoparticles can successfully grow on the surfaces of SMM giving the microspherical shape and microporous structure. The effects of different adsorbents, solution concentration, temperature, and pH value on the adsorption performance were investigated, and the adsorption isotherm and kinetics were analyzed through the adsorption results. The ZIF-9@SMM for removing Congo red from water exhibited better adsorption performance than the ZIF-9, SMM and some other adsorbents. The excellent adsorption performance of ZIF-9@SMM indicated that the fabrication of *in situ* growth method is attractive to be applied for other novel composite adsorbents combining microporous materials and macroporous microspheres.

1. Introduction

Water pollution from textile, pulp, chemical and other industries is a global challenge to environmental protection. Azo dyes widely present in the wastewater of textile industries are harmful to human beings and animals. It has been confirmed that the toxicities of azo dyes can lead to cancer and respiratory diseases.[1,2] Therefore, it is necessary to remove azo dyes from water to avoid harmful impact derived from azo dyes.

Various types of water-treatment techniques, including adsorption,[3] coagulation,[4] membrane filtration,[5] microbial degradation[6–8] and chemical oxidation,[8–10] can be used to remove dyes from wastewater. Compared with other techniques, adsorption treatments generally considered to be highly promising, owing to the simple operation, low cost, high efficiency and convenience. The reported adsorbents for dye removal includes activated carbon,[11] cross-linked cellulose dialdehyde,[12] zinc oxide,[1] calcium hydroxyl apatite,[9] cuprous oxide,[8] and agricultural wastes.[13] Although these adsorbents have a certain adsorption effect, it needs to design novels adsorbents showing the improvement in adsorptive efficiency and adsorption capacity.

Metal–organic frameworks (MOFs), a novel class of porous crystalline materials assembled from metal ions clusters and organic linkers, have attracted great interest in liquid adsorption applications, such as the removal of dyes,[14–18] heavy metals,[19–22] phenol,[23,24] and other hazardous materials.[25–28] The good adsorption performance of MOFs is mainly due to the large pore volumes, structure design ability, high surface areas, and the high amount and dispersity of metal ions in the framework.[29–31] Zeolitic imidazolate frameworks (ZIFs) as a class of MOFs exhibit unique properties of the microporosity, crystallinity, high surface area, and high chemical and thermal stability.[32–35] Recently, ZIFs has attracted considerable attention in adsorption applications for removing hazardous materials from liquid mixtures.[14,23] It has been reported that ZIF-67 has been used as an adsorbent for adsorbing malachite green and the adsorption capacity was as high as 2430 mg g^{-1} at 20 °C.[2] In addition, ZIF-67 was found to adsorptive remove phenol from aqueous system.[23] ZIF-8 can be also used an efficient and stable adsorbent to remove dye, humic acid, arsenate, benzotriazoles from water.[29,30,36,37]

ZIF-9 [Co(benzimidazole)$_2$·2H$_2$O], a kind of ZIFs, is constructed from benzimidazole organic ligands and Co^{2+} ions, establishing a three dimensional microporous metal–organic networks. To our best knowledge, few studies have been done to evaluate the ZIF-9 potential for adsorptive applications. However, the good removal performance of ZIF-9 for removing azo dyes from water can be expected, because of the significant host–guest interactions between ZIF-9 and azo dye molecules. There are the π–π stacking interactions between the benzimidazole (H-PhIM) molecules of ZIF-9 and the aromatic rings of azo

[a]*Beijing Key Laboratory of Lignocellulosic Chemistry, Beijing Forestry University, Beijing, 100083, China. E-mail: wangly@bjfu.edu.cn*

[b]*MOE Engineering Research Center of Forestry Biomass Materials and Bioenergy, Beijing Forestry University, Beijing, 100083, China. E-mail: ljd2012@bjfu.edu.cn*

† Electronic supplementary information (ESI) available: The pseudo-first-order kinetics and pseudo-second-order kinetics fitting results (the $\ln(q_e - q_t)$ as a function of t in Fig. S1 and the t/q_t as a function of t in Fig. S2). See DOI: 10.1039/c6ra26763g

dye molecules, and the electrostatic interactions between the Co^{2+} ions of ZIF-9 and the charged groups of azo dye molecules.

Even ZIF-9 may show good adsorption performance, the hydrophilicity, non-spherical morphologies and aggregated nanoparticles of ZIF-9 are not ideal for efficient adsorption applications of removing azo dyes from water. It is necessary to produce spherical adsorbents based on ZIF-9. Polyacrylate carboxyl super-macroporous microspheres (SMM) is a new kind of microsphere materials with an average grain size of 10 μm and pore size of 500 Å. The large specific surface area, high load capacity, outstanding chemical and mechanical stability of SMM is helpful to apply SMM in adsorption applications. Moreover, the functional groups (carboxyl and hydroxyl groups) of polyacrylate carboxyl materials make the SMM can be modified through surface modifications.

Herein, we firstly reported that a novel spherical adsorbent of ZIF-9 nanoparticles growing on SMM via in situ growth method. Based on the coordination effect between positively charged Co^{2+} of ZIF-9 and negatively charged carboxyl groups (–COO$^-$) of SMM, the Co^{2+} ions can be firstly linked with SMM; and then the SMM having Co^{2+} ions can continually react with H-PhIM molecules, resulting in ZIF-9 crystals specifically anchored on the surfaces of SMM (as shown in Fig. 1).[38] So the as-synthesized ZIF-9@SMM has a microspherical shape similar to SMM and also has the ZIF-9 properties. In this study, we characterized the structural properties of ZIF-9@SMM, and investigated the adsorption performance of ZIF-9, SMM and ZIF-9@SMM for removal of Congo Red (CR, an anionic diazo dye) from water.

2. Experimental section

2.1 Materials and synthesis

The solvents and chemicals used in this study are all commercially available and directly used without further

purification. ZIF-9@SMM was synthesized by the situ growth method as follow (as illustrated in Fig. 1): 1.91 g cobalt nitrate hexahydrate (Co(NO$_3$)$_2$·6H$_2$O) were first dissolved in 200 mL N,N'-dimethylformamide (DMF) in a 500 mL Erlenmeyer flask containing 1.0 g SMM, stirring at 30 °C, 150 rpm of temperature oscillator for 24 h to allow the conjugation of Co^{2+} to –COO$^-$. Then 100 mL DMF solution of H-PhIM (8.5 g) was added into the Co^{2+} solution containing SMM. After reaction for 24 h, the ZIF-9@SMM products were collected by low speed centrifugation and washed repeatedly with ethanol. The as-synthesized products were dried at 80 °C in the vacuum oven for 24 h to obtain the final product, ZIF-9@SMM. In addition, the formulation and synthesis conditions of ZIF-9 were the same as the synthesis of ZIF-9@SMM, but not adding SMM. ZIF-9 was collected by high speed centrifugation after reaction and washed repeatedly with ethanol. The ZIF-9 products were dried at 80 °C in the vacuum oven for 24 h to obtain ZIF-9.

2.2 Characterization experiments

The morphologies of the ZIF-9, SMM and ZIF-9@SMM samples were observed by a scanning electron microscope (SEM, HITACHI SU8010). The crystalline structure of the ZIF-9, SMM and ZIF-9@SMM samples were characterized by powder X-ray diffraction (XRD, Bruker D8 ADVANCE) with Cu-Kα and wavelength of 1.5418 Å in the angle range of 5–50°. The nitrogen adsorption isotherms of the ZIF-9, SMM and ZIF-9@SMM samples were measured by a gas sorption instrument (Micromeritics ASAP 2020) at 77 K, and the surface area was calculated by the Brunauer–Emmett–Teller (BET) method.

2.3 Adsorption experiments

To study the adsorption isotherm, 10 mL CR aqueous solution with different concentrations (from 5 to 250 mg L^{-1}) were
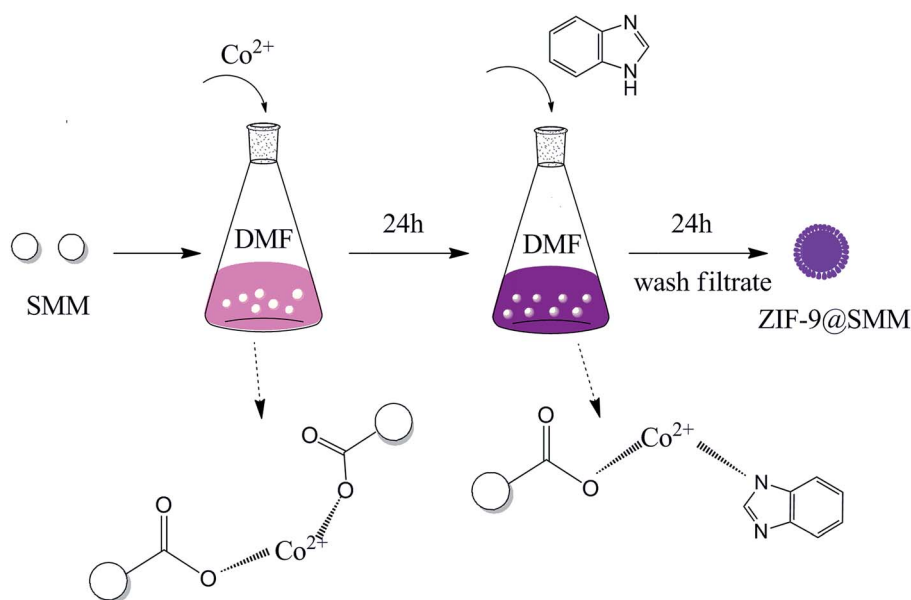

Fig. 1 Illustration of the procures for synthesizing ZIF-9@SMM.

poured into 10 mL centrifugal tubes containing 10.0 mg of ZIF-9, SMM and ZIF-9@SMM samples, and then kept in a thermostatic incubator shaker (HZQ-X100) with a shaking speed of 150 rpm at 30 °C unless otherwise stated. After adsorption for 12 h, the mixture was filtered with a 0.22 μm microporous membrane to collect the dilute solution and to measure the CR concentration.

To study the adsorption kinetics of ZIF-9@SMM, 10 mL CR solution of a fixed initial concentration was added into a 10 mL centrifugal tube containing 10.0 mg ZIF-9@SMM samples, and then placed in a thermostatic incubator shaker (HZQ-X100) with a shaking speed of 150 rpm at 30 °C. After adsorption for a predetermined time (from 20 to 720 min), the dilute solution was collected and was treated in the same manner as described above.

To study the effects of adsorption temperature and pH values on adsorption capacity of CR on ZIF-9@SMM, the adsorption measurements were performed at three different temperatures (20, 30 and 40 °C) and different pH values (from 3 to 9) of CR solutions adjusted by dilute HCl (0.1 M) or NaOH (0.1 M).

The CR concentration was measured by a UV-Vis spectrometer (UV759CRT, Shanghai) at the maximum absorbance of CR dye (496 nm) on the basis of Beer–Lamber law. The amount of adsorption at time t, q_t (mg g^{-1}), was calculated by the eqn (1); and the removal efficiency ($R\%$) was calculated by the eqn (2):

$$q_t = \frac{(C_0 - C_t)V}{m} \tag{1}$$

$$R\% = \frac{(C_0 - C_t)}{C_0} \times 100\% \tag{2}$$

where C_0 and C_t (mg L^{-1}) are the CR concentrations at initial and time t, respectively; V (L) is the volume of the solution; m (g) is the mass of adsorbent used. When the equilibrium adsorption reached, the adsorption capacity at a nearly constant value is the equilibrium adsorption capacity (q_e, mg g^{-1}).

3. Results and discussion

3.1 Characterization results

The XRD patterns of the ZIF-9, SMM and ZIF-9@SMM samples were shown in Fig. 2. The red curve showed the XRD pattern of ZIF-9, which agrees well with the simulated XRD pattern of ZIF-9 according to the published crystal structure data,[39,40] meaning the successful preparation of ZIF-9. The XRD pattern of the SMM sample had three wide peaks, due to the non-crystalline structure of polyacrylate carboxyl. The XRD pattern of ZIF-9@SMM is similar to that of SMM, and also had some additional characteristic peaks matching the ZIF-9 crystalline structure. The observation of the ZIF-9 structure originate from ZIF-9@SMM indicated that the ZIF-9@SMM synthesized through the *in situ* method is a composite product having ZIF-9 crystals loading on the SMM.

The nitrogen adsorption isotherms of the ZIF-9, SMM and ZIF-9@SMM samples measured at 77 K were shown in Fig. 3. The type I isotherms of ZIF-9 having a rapid increase of gas uptake at low relative pressure suggests the presence of
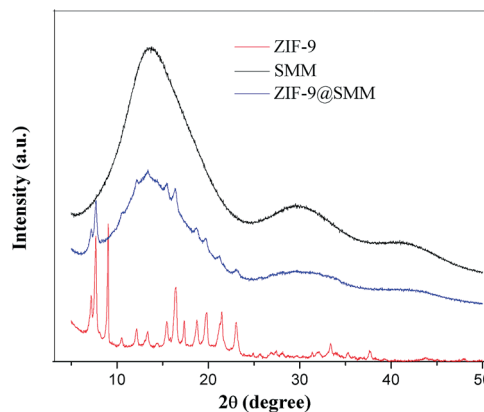

Fig. 2 XRD patterns of the ZIF-9, SMM and ZIF-9@SMM samples.

micropores. On the contrary, the presence of micropores cannot be observed through the nitrogen adsorption isotherms of SMM, because of its super-macroporous structure. The specific surface areas of the ZIF-9, SMM and ZIF-9@SMM calculated by the BET method were 413.0 m^2 g^{-1}, 2.3 m^2 g^{-1} and 31.0 m^2 g^{-1}, respectively. It notes that the BET surface area of the ZIF-9@SMM increases to about 13.5 times of that of the SMM. Therefore, the ZIF-9@SMM may have a microporous structure, which confirms the presence of the microporous ZIF-9 in ZIF-9@SMM.

Fig. 4 showed the SEM images of ZIF-9, SMM and ZIF-9@SMM samples. It can be seen from Fig. 4a that ZIF-9 nanoparticles have a uniform particle size around 100 nm in diameter. The ZIF-9 nanoparticles exhibited similar morphology to the ZIF-9 crystals as reported in literature.[41] The SEM images of SMM in Fig. 4b and c showed a microspherical shape of SMM and the surface pore size was about 50 nm. As seen in Fig. 4d, the as-synthesized ZIF-9@SMM kept the spherical shape after the SMM modified through the *in situ* method. Moreover, Fig. 4e showed that the porous surface of SMM was covered by nanoparticles, and these nanoparticles had the same morphology as the ZIF-9 nanoparticles (Fig. 4a). It indicated that the ZIF-9 nanoparticles successfully grow onto the surfaces of SMM.
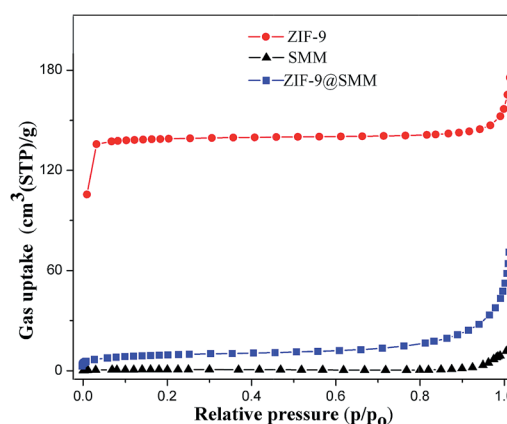

Fig. 3 Nitrogen adsorption isotherms of ZIF-9, SMM and ZIF-9@SMM at 77 K.
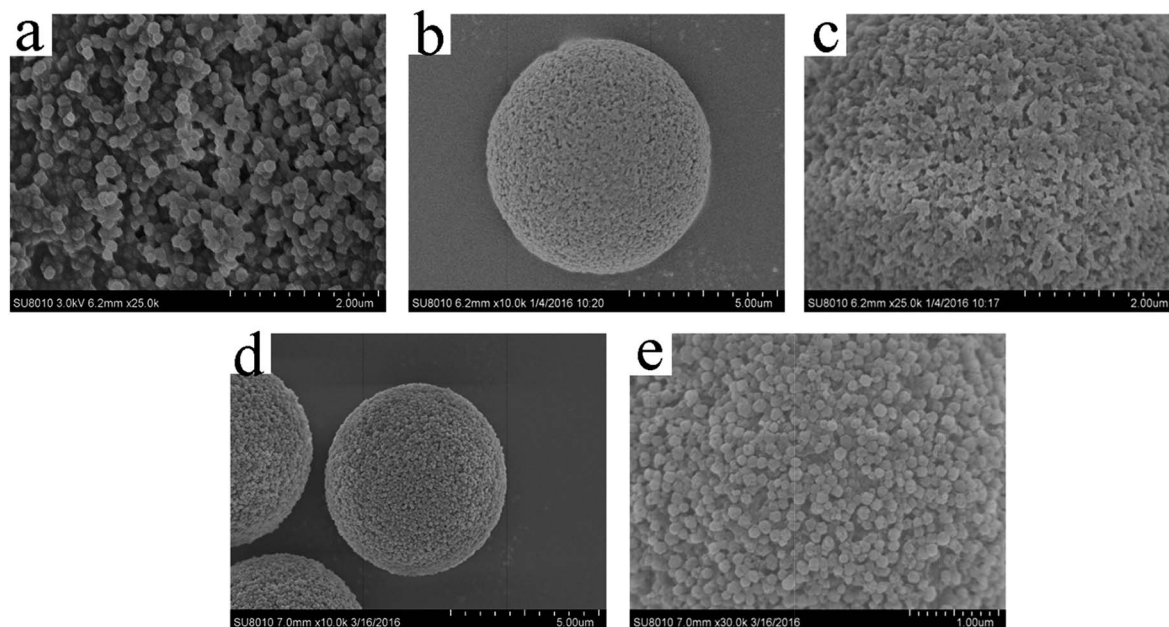
Fig. 4   SEM images of (a) ZIF-9, (b and c) SMM and (d and e) ZIF-9@SMM.

3.2   Adsorption results

As mentioned above, the ZIF-9 nanoparticles growing on the surfaces of the SMM contributes to the ZIF-9@SMM having ZIF-9 properties, which may play an important role in the adsorption of guest species. Thus the ZIF-9@SMM may have significantly different adsorption behaviors with the SMM. CR was used as an anionic azo dye to evaluate the adsorption performances of the ZIF-9, SMM and ZIF-9@SMM under the same conditions. Fig. 5a showed the adsorption isotherms of different adsorbents at the initial CR concentration ranged from 5 to 250 mg L^{-1}. For a 12 h adsorption, the adsorption capacity of each adsorbent gradually increased with increasing the initial concentration, and the increase rate was higher at

lower initial concentration than at higher initial concentration. When the maximal adsorption capacity of an adsorbent almost reached, continually increasing the initial concentration could not significantly increase the adsorption capacity. Therefore, each adsorbent exhibited a slow incensement in adsorption capacity when the initial CR concentration is higher than 75 mg L^{-1}.

In addition, the adsorption capacities of the ZIF-9, SMM and ZIF-9@SMM were similar at the CR concentration of 5 mg L^{-1}. While, the adsorption capacity was obviously in an order of SMM < ZIF-9 < ZIF-9@SMM at the CR concentration higher than 50 mg L^{-1}. The adsorption capacities of SMM, ZIF-9 and ZIF-9@SMM were 18.5 mg g^{-1}, 43.6 mg g^{-1} and at the CR
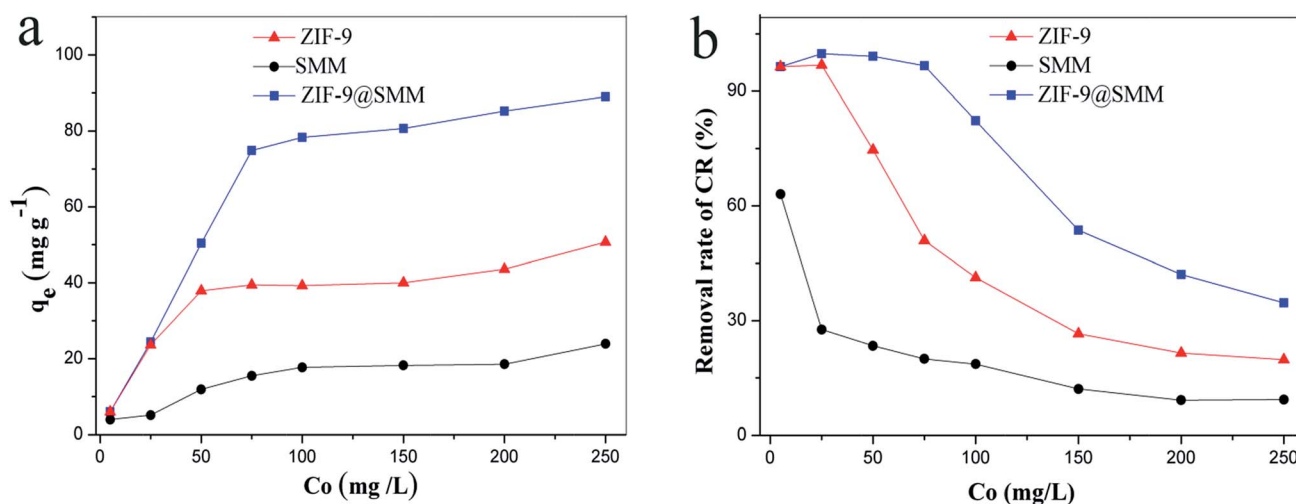

Fig. 5   (a) Adsorption capacity and (b) removal rate of CR on ZIF-9, SMM and ZIF-9@SMM at different initial concentrations (adsorption time: 12 h, adsorption temperature: 30 °C).
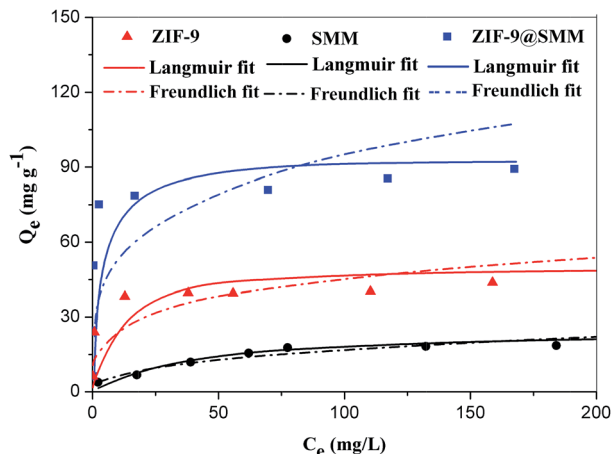
Fig. 6 Adsorption isotherms of CR onto ZIF-9, SMM and ZIF-9@SMM (adsorption time: 12 h, adsorption temperature: 30 °C).
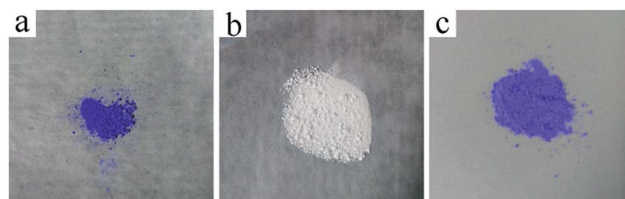

Fig. 7 Photos of the (a) ZIF-9, (b) SMM and (c) ZIF-9@SMM samples before adsorbing CR.

Fig. 8 Photos of the (a) ZIF-9, (b) SMM and (c) ZIF-9@SMM samples after adsorbing CR.

concentration of 200 mg L^{-1}, respectively. Clearly, the ZIF-9@SMM had the maximum adsorption capacity (85.3 mg g^{-1}), which was about 1.0 and 3.6 times higher than the adsorption capacities of the ZIF-9 and SMM, respectively.

The removal rate of CR to different adsorbents (the SMM, ZIF-9 and ZIF-9@SMM) can be seen in Fig. 5b. Consistent with the adsorption isotherms, the order of the removal rate for three adsorbents was SMM < ZIF-9 < ZIF-9@SMM. With increasing the CR concentration from 5 to 250 mg L^{-1}, the removal rate of each adsorbent decreased gradually. The removal rate of SMM sharply decreased from 60% at 5 mg L^{-1} CR to 20% at 250 mg L^{-1} CR, and the ZIF-9@SMM exhibited the highest removal rate in a range of 45–99%. Especially, the removal rate of ZIF-9@SMM was higher than 85% when the CR concentration was from 5–100 mg L^{-1}, and the highest removal rate reached 99.8% at 25 mg L^{-1}.

To further investigate the adsorption isotherms of CR to the ZIF-9, SMM and ZIF-9@SMM, the adsorption isotherm data was analyzed by the Langmuir isotherm and the Freundlich model using the following equation (eqn (3) and (4)), respectively:

$$\frac{C_e}{q_e} = \frac{1}{K_L q_{max}} + \frac{C_e}{q_{max}} \tag{3}$$

$$\ln q_e = \ln K_F + \frac{1}{n} \ln C_e \tag{4}$$

where C_e (mg L^{-1}) is the equilibrium concentration of CR, q_e (mg g^{-1}) is the equilibrium adsorption capacity of CR. q_{max} (mg g^{-1}) denotes the maximal adsorption capacity and K_L represents

the Langmuir adsorption constant, K_F denotes the Freundlich constant and $1/n$ is the heterogeneity factor of the adsorbent, associated with the surface heterogeneity of adsorbent.

The adsorption isotherm data with fitting models were shown in Fig. 6. Higher correlation coefficients of R_L^2 (listed in Table 1) suggested that the Langmuir model is more suitable for describing CR adsorption onto ZIF-9 and ZIF-9@SMM, and the value of R_L^2 of SMM is similar to R_F^2. As shown by SEM images in Fig. 4, the ZIF-9 nanoparticles uniformly grew on the porous surface of the SMM. The pore size of ZIF-9 was significantly smaller than the molecule size of CR, so the CR adsorption was mainly affected by the ZIF-9 nanoparticles on the outer of the ZIF-9@SMM. Therefore, the ZIF-9@SMM exhibited the same Langmuir isotherm mechanism as the ZIF-9. Moreover, the maximum removal capacity of ZIF-9@SMM from the Langmuir model was 90.91 mg g^{-1}, which was in a good agreement with the actual experiment result of 89.0 mg g^{-1} at 250 mg L^{-1} CR concentration.

Fig. 7 showed the photos of the ZIF-9, SMM and ZIF-9@SMM samples before adsorbing CR, it can be seen that ZIF-9 and ZIF-9@SMM were blue-violet powder and SMM was white powder.

The color of the ZIF-9@SMM can visually prove that the ZIF-9 nanoparticles have been successfully attached on the surface of the SMM. The photos of the ZIF-9, SMM and ZIF-9@SMM samples after adsorption measurements were shown in Fig. 8. In contrast to Fig. 7, the colors of the ZIF-9, ZIF-9@SMM and SMM were changed from blue-violet and white to dark red,

Table 1 Adsorption isotherm model parameters derived from the Langmuir model and the Freundlich model

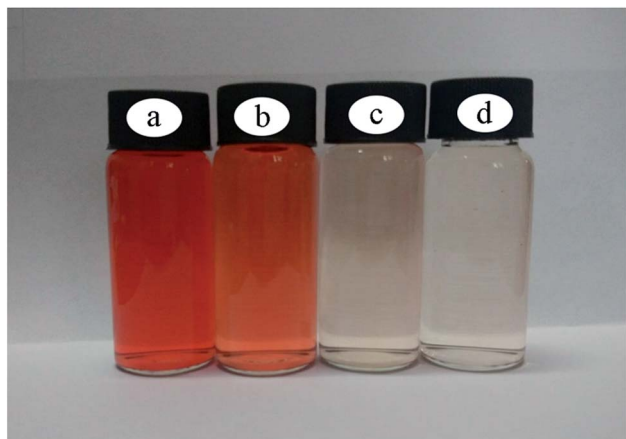| Adsorbents	Langmuir parameters			Freundlich parameters		
	q_m (mg g^{-1})	K_L (L mg^{-1})	R_L^2	K_F (mg g^{-1}) (L mg^{-1})$^{1/n}$	n	R_F^2
ZIF-9	50	0.14	0982	14.92	4.15	0.781
SMM	25	0.03	0.953	2.68	2.53	0.958
ZIF-9@SMM	90.91	0.52	0.998	33.25	4.44	0.545

Fig. 9 Pictures showing the decolorization of CR (100 mg L^{-1}) in the vials using different adsorbents: (a) vials before the addition of adsorbent; (b) vials after the decolorization using SMM microsphere; (c) vials after the decolorization using ZIF-9; (d) vials after the decolorization using ZIF-9@SMM microsphere.
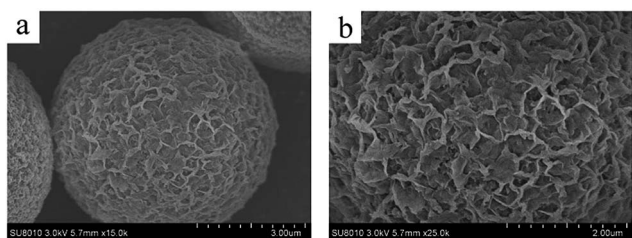

Fig. 10 SEM images of ZIF-9@SMM after CR adsorption (initial CR concentration: 50 mg L^{-1}, adsorption time: 12 h).

reddish purple and light orange, respectively. In addition, Fig. 9 showed the photos of the initial CR solution (100 mg L^{-1}) and three dilute CR solutions adsorbed by the ZIF-9, SMM, ZIF-9@SMM. Compared with Fig. 9a, the colors of the CR solutions adsorbed by different adsorbents all became shallow, and

the red color faded in turn with using SMM, ZIF-9, ZIF-9@SMM. The changes in the colors of adsorbents and CR solutions both showed that the ZIF-9@SMM had the best adsorption performance because of the dark red color of the used ZIF-9@SMM and the significantly light color of the dilute CR solution. While, the adsorption performance of the SMM is not well. The corresponding adsorption capacities and removal rates of the SMM and ZIF-9@SMM are 39.27 mg g^{-1}, 41.28% and 78.32 mg g^{-1}, 82.33%, respectively.

SEM images of the ZIF-9@SMM after adsorbing CR were shown in Fig. 10. Compared to the unused ZIF-9@SMM (Fig. 4d and e), the outer surface of the ZIF-9@SMM exhibited an uneven layer covering the ZIF-9 nanoparticles which were invisible after the CR adsorption as shown in Fig. 10b. This predicted that a thin layer of the CR molecules were adsorbed on the entire external surface of the ZIF-9@SMM. Then the color of the ZIF-9@SMM is changed from blue-violet to dark red (shown in Fig. 7 and 8).

These results showed that the ZIF-9 can absorb CR molecules from water. The adsorption of ZIF-9 is due to the electrostatic interactions between the anionic sulfonic groups of CR and positively charged Co^{2+} ions of ZIF-9. Moreover, the $\pi-\pi$ interactions between the aromatic rings of the CR and the aromatic imidazole rings of the ZIF-9 also should be considered in the adsorption of the CR on ZIF-9.[42-44] However, the hydrophobicity of ZIF-9 affects its dispersion in aqueous solution. ZIF-9 nanoparticles would agglomerate into larger blocks, so that part of the ZIF-9 nanoparticles could not fully contact with CR molecules. Fig. 5 showed that the ZIF-9@SMM had better performance than the ZIF-9, the adsorption capacity of the ZIF-9@SMM could reach at least 1.8 times of that of the ZIF-9. This is because that the SMM is a spherical adsorbent and the distribution of ZIF-9 on the spherical surface can better contacting with the CR molecules in water, resulting the improved adsorption performance. Compared to the ZIF-9, the ZIF-9@SMM with the ZIF-9 nanoparticles on the SMM surfaces requires less amount of ZIF-9 to reach efficient adsorption performance. In addition, the microspherical shape of the
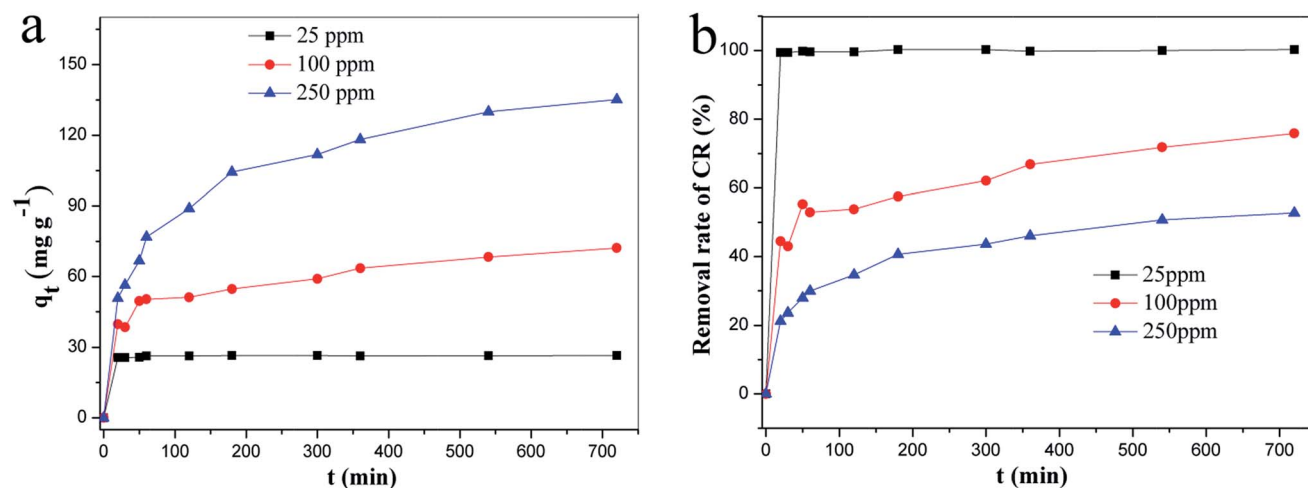

Fig. 11 (a) Adsorption capacity and (b) removal rate of CR on ZIF-9@SMM at different time (adsorption temperature: 30 °C).

Table 2 Kinetic parameters for CR adsorption on ZIF-9@SMM at different initial concentration at 30 °C

Initial concentration ($mg\ L^{-1}$)	Pseudo-first-order kinetic model			Pseudo-second-order kinetic model		
	q_e ($mg\ g^{-1}$)	k_1 (min^{-1})	R^2	q_e ($mg\ g^{-1}$)	k_2 ($g\ (mg^{-1}\ min^{-1})$)	R^2
25	0.57	0.004	0.709	27.03	0.0460	1.000
100	32.73	0.003	0.960	76.92	0.0003	0.992
250	87.72	0.005	0.982	142.86	0.0001	0.995

ZIF-9@SMM is helpful to make it as chromatographic fillers to expand its further application.

To continually investigated the adsorption performance of the ZIF-9@SMM, the time-dependent adsorption properties were studied at three different initial concentrations (25, 100, and 250 mg L^{-1}). Fig. 11 showed the adsorption equilibrium can be reached with increasing the adsorption time. At the initial CR concentration of 25 mg L^{-1}, the adsorption equilibrium was almost reached after a 20–30 min adsorption indicating the excellent adsorption performance of the ZIF-9@SMM for rapidly removing CR. The fast adsorption equilibrium was also found by using ZIF-8/ZIF-67 nanoparticles as adsorbents for removing contaminants from water.[2,30] With increasing the initial CR concentration, the required adsorption time to reach an equilibrium status became longer. A 6 h adsorption cannot well reach the adsorption equilibrium at 100 mg L^{-1} and 25 mg L^{-1} CR concentrations.

As shown in Fig. 11a, the adsorption capacity of the ZIF-9@SMM increased with the initial CR concentration. The maximum adsorption capacity was 146 mg g^{-1} the initial CR concentration of 250 mg L^{-1}, which was 0.9 and 4.6 times higher than at the other two concentrations (100 mg L^{-1} and 25 mg L^{-1}) respectively. The removal rates of CR at different initial concentrations (25, 100 and 250 mg L^{-1}) can be seen in Fig. 11b. The removal rate first increased rapidly and then tended to increase slowly after the gradual increase. The order of the removal rates at 25, 100 and 250 mg L^{-1} CR concentrations was: 25 mg L^{-1} > 100 mg L^{-1} > 250 mg L^{-1}.

It is noted that the removal rates of CR were all close to 100% at the initial CR concentration of 25 mg L^{-1}, indicating most CR molecules can be rapidly removed through a short adsorption time of only 20 min. The ZIF-9@SMM showing the fast and excellent adsorption is mainly caused by the strong electrostatic interactions between the anionic sulfonic groups of CR and positively charged Co^{2+} ions of ZIF-9 and the π–π interactions between the aromatic structures of CR and ZIF-9.

To further analyze the adsorption kinetics, the pseudo-first-order equation and the-pseudo-second-order equation were employed to model the kinetic data in Fig. 11a. The pseudo-first-order and pseudo-second-order equations are typically described in the following two equations (eqn (5) and (6)), respectively:

$$\ln(q_e - q_t) = \ln q_e - k_1 t \tag{5}$$

$$\frac{t}{q_t} = \frac{1}{k_2 q_e^2} + \frac{t}{q_e} \tag{6}$$

where q_t (mg g^{-1}) and q_e (mg g^{-1}) are the adsorption capacities at any time and equilibrium, respectively. k_1 (min^{-1}) represents the pseudo first order rate constant. k_2 (g (mg^{-1} min^{-1})) represents the pseudo second order rate constant.

The fitting results of the adsorption kinetics for CR adsorption using ZIF-9@SMM at different CR concentrations were shown in Fig. S1† (the ln($q_e - q_t$) as a function of t) and Fig. S2† (the t/q_t as a function of t). Table 2 showed the kinetic parameters derived from the linear regressions of the fitting results (shown in Fig. S1 and 2†). For pseudo-first-order fitting, the
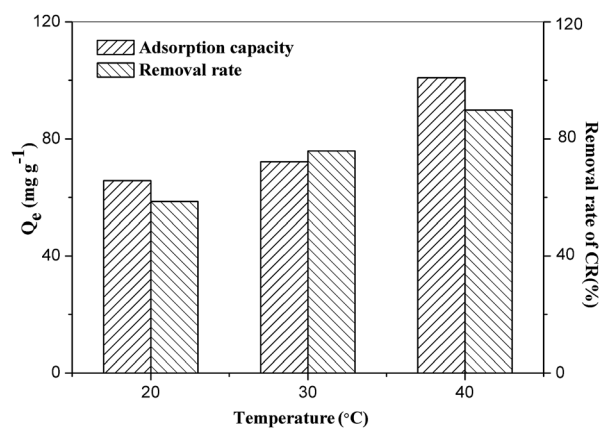

Fig. 12 Effects of adsorption temperature on adsorption capacity and removal rate of CR on ZIF-9@SMM (adsorption time: 12 h, initial concentration: 100 mg L^{-1}).
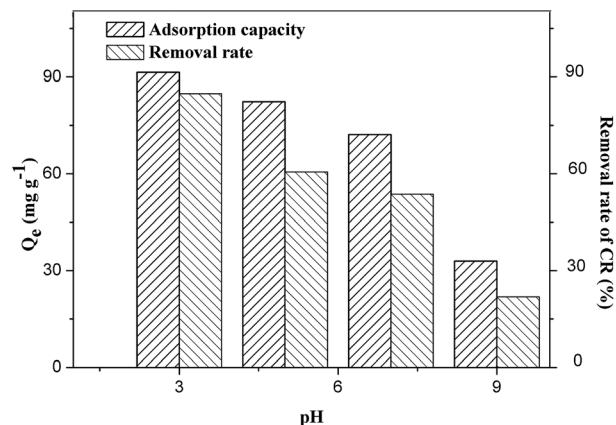

Fig. 13 Effects of pH on adsorption capacity and removal rate of CR on ZIF-9@SMM (adsorption time: 12 h, adsorption temperature: 30 °C, initial concentration: 100 mg L^{-1}).
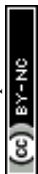
Table 3 Comparison of different adsorbents for CR adsorption capacities

Adsorbent	Initial concentration (mg L^{-1})	Adsorbents dosage (g L^{-1})	Adsorption capacity (mg g^{-1})	Reference
ZIF-9@SMM	250	1	146	In this study
Coir pith	20	18	6.72	46
Sugarcane bagasse	500	10	38.2	47
Bentonite	1000	20	35.84	48
Kaolin	150	50	5.44	48
Chitosan hydrobeads	500	4	92.59	49
Fly ash	100	10	4.13	50
Leaf powder	40	1	41.2–28.3	51
Bael shell carbon	50	1	98.04	52

higher the concentration the more consistent, the value of R^2 increased from 0.709 to 0.982 at the concentration range of 25–250 mg L^{-1}. However, the pseudo-second-order fitting showed that the three R^2 values were all close to 1 and higher than the pseudo-first-order fitting at each CR concentration. The better correlation fittings indicated that the experimental adsorption kinetics of the ZIF-9@SMM for CR removal well accorded with the pseudo-second-order model. Therefore, the adsorption behaviour of the ZIF-9@SMM is dominated by the surface properties of the ZIF-9@SMM and the CR concentrations in solutions.

Besides of the initial CR concentration, the adsorption capacity of the ZIF-9@SMM is also affected by the adsorption temperature and pH values. As can be seen from Fig. 12, the adsorption capacity and removal rate gradually increased with increasing the adsorption temperature. When the temperature increased from 20 to 30 °C, the adsorption capacity increased 6.47 mg g^{-1}, and when the temperature continued to increase 10 °C, the adsorption capacity increased 28.68 mg g^{-1}.

This indicated that the higher the temperature the better the adsorption capacity of the ZIF-9@SMM, which may because that the CR molecules could exist in the gaps between ZIF-9 nanoparticles and/or enter in the pores of the SMM.

Fig. 13 showed the effects of pH on the adsorption properties (adsorption capacity and removal rate) of the ZIF-9@SMM. Since the typical pH range of wastewater and aquacultural wastewater is from 4 to 9,[2] the pH range was carried out from 3 to 9 in this study. According to the adsorption studies of ZIF-8, the surface positive charges of ZIF-8 gradually decreased to become negative charges in the pH range from 3 to 9.[30,36] Since ZIF-9 and ZIF-8 are similar in the framework structures, the surface positive charges of ZIF-9 should decrease as the pH value rises. Therefore, the adsorption performance declined with increasing pH value due to the decrease in the electrostatic interactions between the anionic CR and positively charged ZIF-9. It was found that the adsorption capacities for CR decreased more significantly when pH = 9, which is 36% of adsorption capacity at pH = 3. This may be caused by the fact that the surface charge of ZIF-9 would change from positive to neutral or even negative at pH = 9. The OH$^-$ ions in the CR solution at pH > 7 also can result in the decreased adsorption properties of the ZIF-9@SMM, because the OH$^-$ ions may compete with the negatively charged CR molecules when interacting with the positively charged Co^{2+} ions of ZIF-9.[45] The decrease in the adsorption capacity with increasing pH indicated that the CR adsorption of the ZIF-9@SMM is more affected by the electrostatic interactions. When the electrostatic interactions become weak, the high adsorption capacity cannot be maintained even if there are still π–π interactions. Therefore, the ZIF-9@SMM is more suitable for as an adsorbent to remove CR from wastewater at lower pH values.

The reported adsorbents for removing CR from water and the maximum adsorption capacities were shown in Table 3. The maximum adsorption capacity of ZIF-9@SMM on CR is 146 mg g^{-1}, it could be up to 1.5 times or even 35 times that of bael shell carbon or fly ash. Compared with most of these adsorbents having irregular shapes, the ZIF-9@SMM is a new type of spherical adsorbents and thus can be further applied in chromatography applications. In addition, the synthesis methods of ZIF-9@SMM only need to operate at room temperature conditions, simple and convenient, and its size can be directly controlled by changing the size of the ball. It can be expected that the ZIF-9@SMM has a great potential to other adsorption applications.

4. Conclusions

In this study, the ZIF-9@SMM with ZIF-9 nanoparticles growing on the porous surface of SMM was successfully synthesized by *in situ* growth method, which had both the microspherical shape of SMM and the microporous structure of ZIF-9. The adsorption capacities of SMM, ZIF-9 and ZIF-9@SMM were 18.5 mg g^{-1}, 43.6 mg g^{-1} and 85.3 mg g^{-1} respectively, after adsorbing 200 mg L^{-1} CR for 12 h. Moreover, the ZIF-9@SMM can quickly reach high adsorption capacities, especially at the low initial concentration of the CR solution. The adsorption mechanism of the ZIF-9@SMM includes the interactions the electrostatic interaction between the anionic sulfonic groups of CR and positively charged Co^{2+} ions of ZIF-9 and the π–π interaction between the aromatic rings of CR and the aromatic imidazole rings of ZIF-9. Compared with the pure ZIF-9, the significantly improved adsorption performance of ZIF-9@SMM is due to the spherical ZIF-9@SMM helping the hydrophobic ZIF-9 to fully contact with the CR molecules. The ZIF-9@SMM can be a promising adsorbent to remove dye or other contaminants from water, and its microspherical shape may make it as a chromatographic filler to further expand its application.

Acknowledgements

Notes and references

1 N. Güy, S. Çakar and M. Özacar, *J. Colloid Interface Sci.*, 2016, **466**, 128–137.

2 K.-Y. A. Lin and H.-A. Chang, *Chemosphere*, 2015, **139**, 624–631.

3 A. Mittal, J. Mittal, A. Malviya and V. Gupta, *J. Colloid Interface Sci.*, 2009, **340**, 16–26.

4 G. Sen, S. Ghosh, U. Jha and S. Pal, *Chem. Eng. J.*, 2011, **171**, 495–501.

5 S. E. Elaigwu, V. Rocher, G. Kyriakou and G. M. Greenway, *J. Ind. Eng. Chem.*, 2013, **20**, 3467–3473.

6 I.-S. Ng, T. Chen, R. Lin, X. Zhang, C. Ni and D. Sun, *Appl. Microbiol. Biotechnol.*, 2014, **98**, 2297–2308.

7 K. P. Gopinath, S. Murugesan, J. Abraham and K. Muthukumar, *Bioresour. Technol.*, 2009, **100**, 6295–6300.

8 J. Shu, Z. Wang, Y. Huang, N. Huang, C. Ren and W. Zhang, *J. Alloys Compd.*, 2015, **633**, 338–346.

9 C. Srilakshmi and R. Saraf, *Microporous Mesoporous Mater.*, 2016, **219**, 134–144.

10 Y. Li, A. Meas, S. Shan, R. Yang and X. Gai, *Bioresour. Technol.*, 2016, **207**, 379–386.

11 H. Deng, L. Yang, G. Tao and J. Dai, *J. Hazard. Mater.*, 2009, **166**, 1514–1521.

12 S. Kumari, D. Mankotia and G. S. Chauhan, *J. Environ. Chem. Eng.*, 2016, **4**, 1126–1136.

13 H. Wang, X. Yuan, G. Zeng, L. Leng, X. Peng, K. Liao, L. Peng and Z. Xiao, *Environ. Sci. Pollut. Res.*, 2014, **21**, 11552–11564.

14 R. Chandra, S. Mukhopadhyay and M. Nath, *Mater. Lett.*, 2016, **164**, 571–574.

15 M. Roushani and Z. Saedi, *J. Taiwan Inst. Chem. Eng.*, 2016, **66**, 164–171.

16 E. Haque, J. E. Lee, I. T. Jang, Y. K. Hwang, J.-S. Chang, J. Jegal and S. H. Jhung, *J. Hazard. Mater.*, 2010, **181**, 535–542.

17 E. Haque, J. W. Jun and S. H. Jhung, *J. Hazard. Mater.*, 2011, **185**, 507–511.

18 E. Haque, V. Lo, A. I. Minett, A. T. Harris and T. L. Church, *J. Mater. Chem.*, 2014, **2**, 193–203.

19 A. Abbasi, T. Moradpour and K. Van Hecke, *Inorg. Chim. Acta*, 2015, **430**, 261–267.

20 D. Chen, W. Shen, S. Wu, C. Chen, X. Luo and L. Guo, *Nanoscale*, 2016, **8**, 7172–7179.

21 A. Jamali, A. A. Tehrani, F. Shemirani and A. Morsali, *Dalton Trans.*, 2016, **45**, 9193–9200.

22 E. Rahimi and N. Mohaghegh, *Mine Water Environ.*, 2016, **35**, 18–28.

23 Y. Pan, Z. Li, Z. Zhang, X.-S. Tong, H. Li, C.-Z. Jia, B. Liu, C.-Y. Sun, L.-Y. Yang and G.-J. Chen, *J. Environ. Manage.*, 2016, **169**, 167–173.

24 B. N. Bhadra, I. Ahmed and S. H. Jhung, *Fuel*, 2016, **174**, 43–48.

25 B. Van de Voorde, B. Bueken, J. Denayer and D. De Vos, *Chem. Soc. Rev.*, 2014, **43**, 5766–5788.

26 N. A. Khan and S. H. Jhung, *J. Hazard. Mater.*, 2013, **260**, 1050–1056.

27 I. Ahmed, N. A. Khan and S. H. Jhung, *Inorg. Chem.*, 2013, **52**, 14155–14161.

28 Z. Hasan and S. H. Jhung, *J. Hazard. Mater.*, 2015, **283**, 329–339.

29 H.-P. Jing, C.-C. Wang, Y.-W. Zhang, P. Wang and R. Li, *RSC Adv.*, 2014, **4**, 54454–54462.

30 J. Q. Jiang, C. X. Yang and X. P. Yan, *ACS Appl. Mater. Interfaces*, 2013, **5**, 9837–9842.

31 X. Li, W. Guo, Z. Liu, R. Wang and H. Liu, *Appl. Surf. Sci.*, 2016, **369**, 130–136.

32 K. S. Park, Z. Ni, A. P. Côté, J. Y. Choi, R. Huang, F. J. Uribe-Romo, H. K. Chae, M. O'Keeffe and O. M. Yaghi, *Proc. Natl. Acad. Sci. U. S. A.*, 2006, **103**, 10186–10191.

33 D. Bradshaw, A. Garai and J. Huo, *Chem. Soc. Rev.*, 2011, **41**, 2344–2381.

34 R. Banerjee, A. Phan, B. Wang, C. Knobler, H. Furukawa, M. O'Keeffe and O. M. Yaghi, *Science*, 2008, **319**, 939–943.

35 A. Ahmed, M. Forster, J. Jin, P. Myers and H. Zhang, *ACS Appl. Mater. Interfaces*, 2015, **7**(32), 18054–18063.

36 J. Li, Y.-N. Wu, Z. Li, B. Zhang, M. Zhu, X. Hu, Y. Zhang and F. Li, *J. Phys. Chem. C*, 2014, **118**, 27382–27387.

37 K. Y. A. Lin and H. A. Chang, *Water, Air, Soil Pollut.*, 2015, **226**, 1–17.

38 J. Ma, X. Guo, Y. Ying, D. Liu and C. Zhong, *Chem. Eng. J.*, 2016, DOI: 10.1016/j.cej.2016.10.127.

39 L. T. L. Nguyen, K. K. A. Le, H. X. Truong and N. T. S. Phan, *Catal. Sci. Technol.*, 2012, **2**, 521–528.

40 Z. Öztürk, J. P. Hofmann, M. Lutz, M. Mazaj, N. Z. Logar and B. M. Weckhuysen, *Eur. J. Inorg. Chem.*, 2015, **9**, 1625–1630.

41 M. He, J. Yao, Q. Liu, Z. Zhong and H. Wang, *Dalton Trans.*, 2013, **42**, 16608–16613.

42 M. S. Tehrani and R. Zare-Dorabei, *Spectrochim. Acta, Part A*, 2016, **160**, 8–18.

43 A. Ayati, M. N. Shahrak, B. Tanhaei and M. Sillanpää, *Chemosphere*, 2016, **160**, 30–44.

44 J. Hu, H. Yu, W. Dai, X. Yan, X. Hu and H. Huang, *RSC Adv.*, 2014, **4**, 35124–35130.

45 M. Akgül, *J. Hazard. Mater.*, 2014, **267**, 1–8.

46 C. Namasivayam and D. Kavitha, *Dyes Pigm.*, 2002, **54**, 47–58.

47 Z. Zhang, L. Moghaddam, I. M. O'Hara and W. O. S. Doherty, *Chem. Eng. J.*, 2011, **178**, 122–128.

48 V. Vimonses, S. Lei, J. Bo, C. W. K. Chow and C. Saint, *Chem. Eng. J.*, 2009, **148**, 354–364.

49 S. Chatterjee, S. Chatterjee, B. P. Chatterjee and A. K. Guha, *Colloids Surf., A*, 2007, **299**, 146–152.

50 V. V. B. Rao and S. R. M. Rao, *Chem. Eng. J.*, 2006, **116**, 77–84.

51 K. G. Bhattacharyya and A. Sharma, *J. Environ. Manage.*, 2004, **71**, 217–229.

52 R. Ahmad and R. Kumar, *Appl. Surf. Sci.*, 2010, **257**, 1628–1633.